Concept
doi.org/10.1002/anse.202100032

Chemistry Europe
European Chemical Societies Publishing

www.analysis-sensing.org

Single-Cell Metabolomics by Mass Spectrometry: Opportunities and Challenges

Marjan Dolatmoradi,[a] Laith Z. Samarah,[a] and Akos Vertes*[a]

Cellular heterogeneity is an inherent property of cell populations with a wide spectrum of biological manifestations, ranging from barely observable variations that enhance organismal adaptation, to life-threatening differences. Single-cell metabolomics can reveal molecular information and variations in metabolite concentrations between cells that are masked in cell-population studies. These differences are quantitatively captured by the abundance distributions for the population and their statistical analysis can reveal the presence of latent subpopulations. In recent years, mass spectrometry (MS), combined with novel sampling and ionization techniques, has become an important tool for single-cell metabolomics. These new techniques must contend with significant challenges in the form of small cell sizes and volumes, ultratrace metabolite amounts per cell, and potentially interfering high turnover rates and rapid diffusion. Owing to the ultrasmall sample volume, low abundance of some metabolites, and poor ionization efficiencies, metabolite detection, identification, and accurate quantitation remain a major challenge. The ability of some techniques to analyze tissue-embedded cells opens the door for spatial metabolomics, potentially revealing cellular synergism in organ level metabolism. In this Concept article, we present a bird's eye view of these major themes in single cell metabolomics and some of the relevant MS-based methods.

1. Introduction

Compositional heterogeneity is an inherent property of cell populations, including isogenic populations, that can be manifested in phenotypic differences. Heterogeneity of metabolite levels can stem from stochastic transcription events, the functioning of enzymes with low copy numbers, and random environmental perturbations.[1] Metabolite levels determined by single-cell analysis provide information on the actual functioning of metabolic pathways in the individual cell and it is considered to be the closest molecular readout of cellular phenotypes.[2,3] Capturing population statistics from single-cell measurements, recognizing patterns of heterogeneity, and assessing the functional information of identified patterns are required as a combined approach to study heterogeneity in a biological system.[4]

With high sensitivity, broad molecular coverage, wide dynamic range, and structural identification capabilities, mass spectrometry (MS) is becoming a powerful platform for single-cell metabolomics that allows for the determination of cellular metabolite levels (see Figure 1). Conventional MS-based assays focus on obtaining molecular information from the average response of a cell population, typically involving 10^6 cells, ignoring the unique properties arising from cell-to-cell variations.[5] In single-cell metabolomics, spatiotemporal variations, including cell division, and response to environmental perturbations can be acquired.[6] Single-cell metabolomics can provide relevant information about the phenotypic variations between individual cells. In addition to population-wide heterogeneity, rare cells and hidden subpopulations can also be discovered using single-cell techniques.[7] Cell-to-cell communication, and interactions with other cells can be captured in relation to diseases or specific cellular pathways.[8]

The main challenges in single-cell metabolomics originate from the small linear dimensions and very low volume of a cell (e.g., ~1 pL for a typical mammalian cell, or 0.6 fL for a bacterial cell in Figure 2), large number of biochemical species in low absolute amounts, wide dynamic range of their concentrations, their large structural diversity, high rate of molecular diffusion, and rapid turnover rates.[9] Because of the rapid turnover rates of some metabolites, keeping cells in their native environment (in situ or preferably *in vivo)* during analysis is critical to avoid or mitigate the perturbations caused by chemical and/or physical treatment (external environmental influences).[10–11] Additionally, although a vast ensemble of various cell lines can be cultured in vitro, the metabolic profiles of such cells appear significantly different in vivo.[12]

Because of the small linear dimensions of cells, high-precision cell manipulation platforms are necessary. Depending on cell size and volume, ranging from ~1 μm and 1 fL, respectively, in bacteria to ~50 μm and 1 nL, respectively, in plant cells, different methods are utilized for manipulation. In addition, different tools are required for free floating (circulating) and tissue embedded cells. For example, microfluidics platforms are used for high-throughput single-cell isolation from bulk populations of free floating cells with relatively low perturbation of cell metabolism.[13] In the nanoPOTS technology, used mostly for single cell proteomics, cells isolated by fluorescence-activated cell sorting are chemically processed in nanowells that provide a highly confined volume to avoid unnecessary dilution of the cell content.[14] Tissue embedded mammalian and plant cells can be interrogated by focused ion

[a] *M. Dolatmoradi, Dr. L. Z. Samarah, Prof. Dr. A. Vertes*
Department of Chemistry
The George Washington University
Washington, DC 20052 (USA)
E-mail: vertes@gwu.edu

beams (secondary ion MS, SIMS, and multiplexed ion beam imaging, MIBI) or laser beams (matrix-assisted laser desorption ionization, MALDI, and laser ablation electrospray ionization, LAESI), or capillary microsampling.[15–17]

Specific challenges stem from the MS technology itself. Despite recent progress with respect to sensitivity and mass resolution, putative identification of metabolites based exclusively on accurate masses is often ambiguous, as many ions and ion adducts can have indistinguishable measured masses.[18] Structural isomers further complicate metabolite identification, sometimes leading to misannotation, which cannot be resolved without additional methods, such as high-resolution ion mobility separation (IMS).[19] The ion intensities for individual analytes, even at identical concentrations, can be very different when ionization efficiencies are dissimilar. Furthermore, in-source fragmentation produces unwanted by-products that are identical to ions of other metabolites, and can result in flawed quantitation.[19] In cases where the hunt is on for new compounds, it is critical to distinguish between sample- and background-related species (i.e., artifacts). This, however, can be difficult and may require additional analytical techniques to supplement the findings.

To reveal cellular heterogeneity, MS approaches with sufficiently low limits of detection (LODs) for single-cell metabolomics need to be developed and validated. As some metabolite concentrations are at the low μM level, depending on the cell volume, MS-based approaches with LODs in the range of 1 zmol to 1 amol present suitable analytical platforms for single cells. In this Concept article, we explore the opportunities and challenges for MS methods in single cell metabolomics.

2. Opportunities

2.1. Characterization of cellular heterogeneity and hidden phenotypes

Stochastic variations in biological processes, such as fluctuations in gene expression, enzyme activity and metabolite levels, the stage in the cell-cycle, the number of ribosomes, and the quantity of proteins bring individual characteristics to single cells that cannot be revealed in bulk analysis.[20] In addition, extrinsic parameters including variations in the concentrations of extracellular chemical species can cause cellular heterogeneity.[21] All these variations are reflected in the distributions of abundances, $c_{i,j}$, of the i-th metabolite in the j-th cell throughout the population (see Figure 3) that can be inferred from the corresponding normalized ion intensities, $I_{i,j}$, measured by single-cell MS. For **unimodal distributions**, a quantitative metric of these variations are the metabolic noise values, η_i^2, defined as $\eta_i^2 = \sigma_i^2/\mu_i^2$, where the means, μ_i, and the standard deviations, σ_i, of the abundances are, $\mu_i = \langle c_{i,j} \rangle$ averaged for all cells, and $\sigma_i = \sqrt{\frac{1}{N-1}\sum_{j=1}^{N} \langle \left(c_{i,j} - \langle c_{i,j} \rangle\right)^2 \rangle}$, respectively.

Characterization of **bimodal distributions** relies on deconvolution of the abundance distribution into two components, for example, two normal distributions with separate $\mu_{i,1}$ and $\mu_{i,2}$, and $\sigma_{i,1}$ and $\sigma_{i,2}$ values (see Figure 3b). Establishing clearly separated subpopulations in such cases is not trivial. Multiple statistical criteria have been developed depending on the nature of the underlying subpopulation distributions. For example, for two normal distributions the Ashman's criterium states that $D_i > 2$ is required for their distinction (Equation 1).

Marjan Dolatmoradi received her M.S. degree in computational chemistry from American University in Washington, DC, USA in 2018. In 2019, she joined the research group of Prof. Akos Vertes at the George Washington University. Her current work focuses on single-cell metabolomics using mass spectrometry-based techniques under ambient conditions.

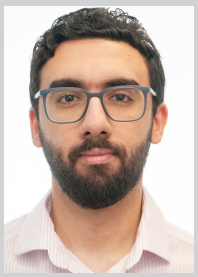

Laith Z. Samarah is a Postdoctoral Research Associate at Princeton University. He received his Ph.D. in chemistry from the George Washington University and his B.S. degree in biology from the American University of Beirut. His doctoral research focused on developing and implementing mass-spectrometry-based methods for single-cell metabolomics and matrix-free molecular imaging of biological tissues. His current research interests include developing mass-spectrometry-imaging methods to map metabolic fluxes at cellular resolution in tissues through in-vivo stable isotope tracing.

Akos Vertes is a Professor of Chemistry and of Biochemistry and Molecular Biology at the George Washington University in Washington, DC, USA. He received his Ph.D. from the Eötvös Loránd University in Budapest, Hungary in 1979. His research interests encompass the development of new analytical techniques. Research areas include single-cell and subcellular analysis, high-throughput methods in systems biology for rapid mechanism-of-action studies, and new methods for molecular imaging of biological tissues under native conditions. He was elected Fellow of the U.S. National Academy of Inventors in 2013.

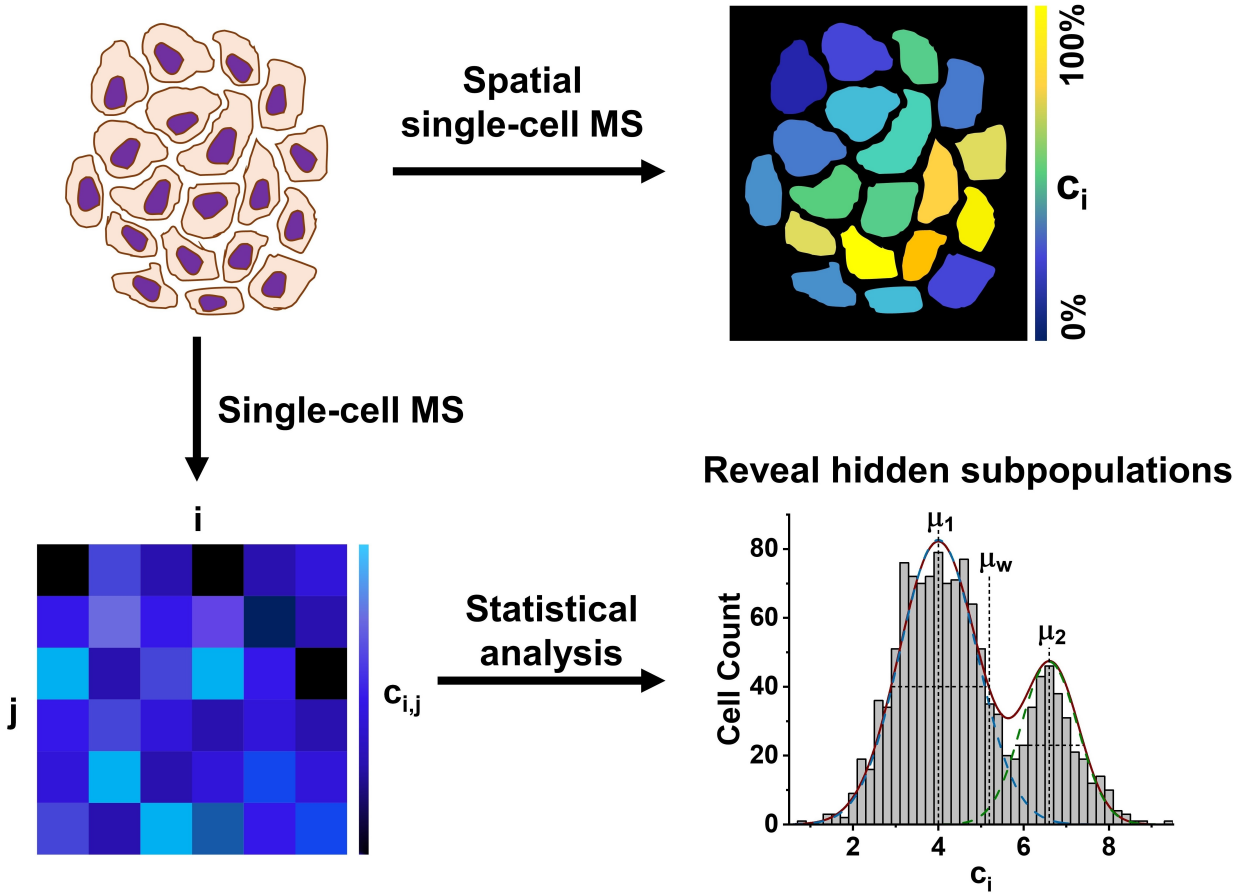

Figure 1. Opportunities in single-cell MS. Metabolite abundances, c_{ij} (bottom left panel), for the *i*-th metabolite in the *j*-th cell, measured by single-cell MS can be statistically analyzed to glean information on the metabolic states of the constituent cell subpopulations. For example, two metabolically distinct subpopulations can be revealed *post hoc* according to the corresponding mean metabolite abundances, μ_1 and μ_2, that differ from the average metabolite abundance for the whole population, μ_w (bottom right panel). In spatial metabolomics, cell location and metabolite abundance information are collected (top right panel).

$$D_i = \frac{\sqrt{2}|\mu_{i,1} - \mu_{i,2}|}{\sqrt{\sigma_{i,1}^2 + \sigma_{i,2}^2}} \quad (1)$$

Metabolic noise can be defined for the subpopulations similarly to the unimodal case, i.e., $\eta_{i,1}^2 = \sigma_{i,1}^2/\mu_{i,1}^2$ and $\eta_{i,2}^2 = \sigma_{i,2}^2/\mu_{i,2}^2$. These subpopulations are often not recognized by any other means, e.g., by color or morphometric differences, and remain hidden.

Post hoc recognition of such biochemical phenotypes can provide new insight into otherwise homogeneous populations. **Identification of** these **latent cellular subtypes (Opportunity 1)**, resulting from upregulation or downregulation of certain biomolecular levels, is enabled by single cell approaches. Chemical classification of cellular subtypes can elucidate cellular specialization, function, or malfunction within a tissue. For example, bimodal metabolite distributions were detected by optical fiber-based laser ablation electrospray ionization MS (f-LAESI-MS) of soybean (*Glycine max*) root nodule cells infected by rhizobia (*Bradyrhizobium japonicum*).[22] For malate, a primary metabolite in plant cells, the bimodal abundance distribution in the nodules was attributed to different malate concentrations in quiescent and dividing bacteroids in the infected plant cells.[22]

Distinct **metabolic states (Opportunity 2) can be manifested** in response to external perturbations. For example, in the left panel of Figure 4 healthy human hepatocytes exhibit high adenylate energy charge, $AEC = 0.82 \pm 0.12$ with low metabolic noise, $\eta^2 = \sigma^2/\mu^2 = 0.021$. Rotenone treatment induces mitochondrial dysfunction resulting in apoptosis characterized by a low energy state, $AEC = 0.16 \pm 0.12$, and high metabolic noise, $\eta^2 = 0.562$.[6] In the right panel of Figure 4, yeast cells exposed to oxidative stress upregulate glutathione, a major redox buffer, compared to control cells raised in regular medium.[23]

Rare cells (Opportunity 3), such as cancer stem cells, circulating tumor cells, etc., **represent minor cell types** in which transcript, protein, or metabolite profiles are significantly different from the rest of the population (see Figure 3c). For this reason, there is no need to deconvolute the overall distribution for the two subpopulations, and the $\mu_{i,1}$, $\mu_{i,2}$, and $\sigma_{i,1}$, $\sigma_{i,2}$ values can be directly calculated. For free floating cells, the combination of enrichment by flow cytometry and metabolomics, adapted for low cell numbers, enables the

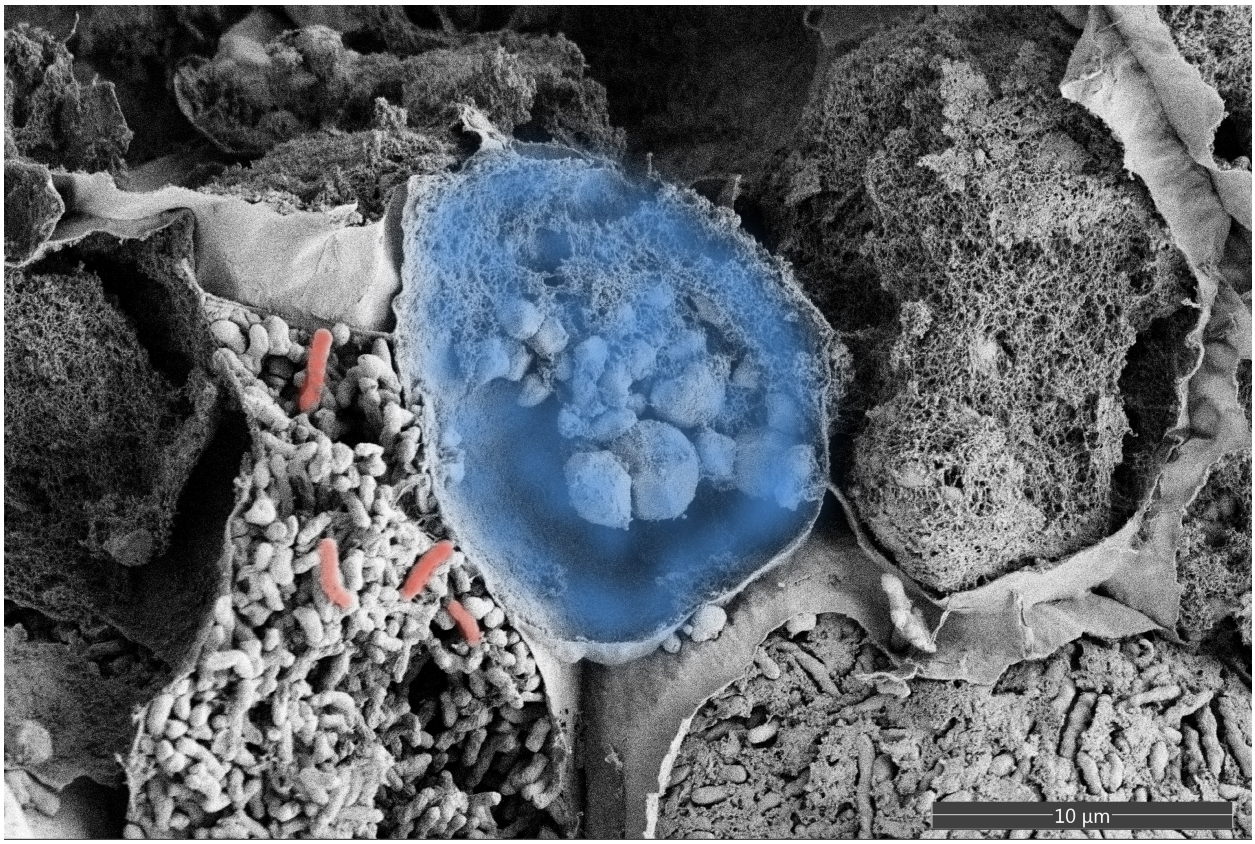

Figure 2. Comparison of cell sizes and volumes for a plant (*G. max* root nodule cell, blue) infected by bacteria (*B. japonicum* cell, red) in a colorized SEM image. The plant cell long and short axes are 16.7 μm and 13.6 μm, respectively, whereas a bacterial cell long and short axes are 2.4 μm and 0.55 μm, respectively. Approximating the cells by cylinders yields 2430 fL and 0.6 fL for their volumes, i.e., the plant cell is ~4000 larger than the bacterial cell in volume.

capture of metabolic profiles for rare cells. For example, the metabolic profiles of rare hematopoietic stem cells (HSCs), isolated by flow cytometry, were obtained using liquid chromatography and orbitrap MS.[24] They found 78 significantly up- or downregulated metabolites for HSCs compared to whole bone marrow cells. At the single cell level, microfluidic enrichment followed by live single cell (LSC) MS yielded metabolomic profiles for circulating tumor cells (CTCs) obtained from 2 cancer types.[25] Compared to lymphocytes, CTCs showed 119 peaks specific to CTCs.

Single cell metabolomic measurements can yield hundreds of spectral features per cell and capture differences that are not manifested in the abundances of a single component. In-depth interpretation of cellular heterogeneity in such high-dimensional data requires dimensionality reduction. The multivariate statistical methods used to extract the underlying cell cluster organization include principal component analysis (PCA), orthogonal projections for latent structures discriminant analysis (OPLS-DA), and for high-dimensional datasets t-distributed stochastic neighborhood embedding (t-SNE), and uniform manifold approximation and projection (UMAP) (see Figure 3d).[26] The latter approaches can **reveal the presence of multiple hidden phenotypes**.

2.2. Cellular genotype vs phenotype

Metabolites are the final downstream products of gene expression that, in principle, connect cellular genotype and phenotype. However, this connection can be significantly altered by environmental and ontogenetic factors. Due to the stochastic fluctuations in biological events arising from the low copy numbers of certain transcripts and proteins, cellular heterogeneity develops even in isogenic cell populations that exist in the same microenvironment. Over time this leads to variations in the cell cycle, and the stage the cell occupies. Among the most visible consequences of phenotypic variations are differences in cellular size and shape. Morphometric cell classification based on image analysis in microscopy in combination with cellular resolution MSI can be used to correlate histological features with metabolic differences.[27]

Thus, **metabolites reflect cellular heterogeneity as they are affected by the integrated influence of gene expression, protein function, and upstream cellular processes (Opportunity 4)**.[28–29] For example, connecting tissue response to drug exposure solely with genotypes may be incomplete, whereas incorporating the corresponding cellular phenotypes can provide information on the relevant molecular pathways that are targeted by the drug. In an early study, using a microarrays for MS (MAMS) platform, phenotypic differences in *S. cerevisiae*

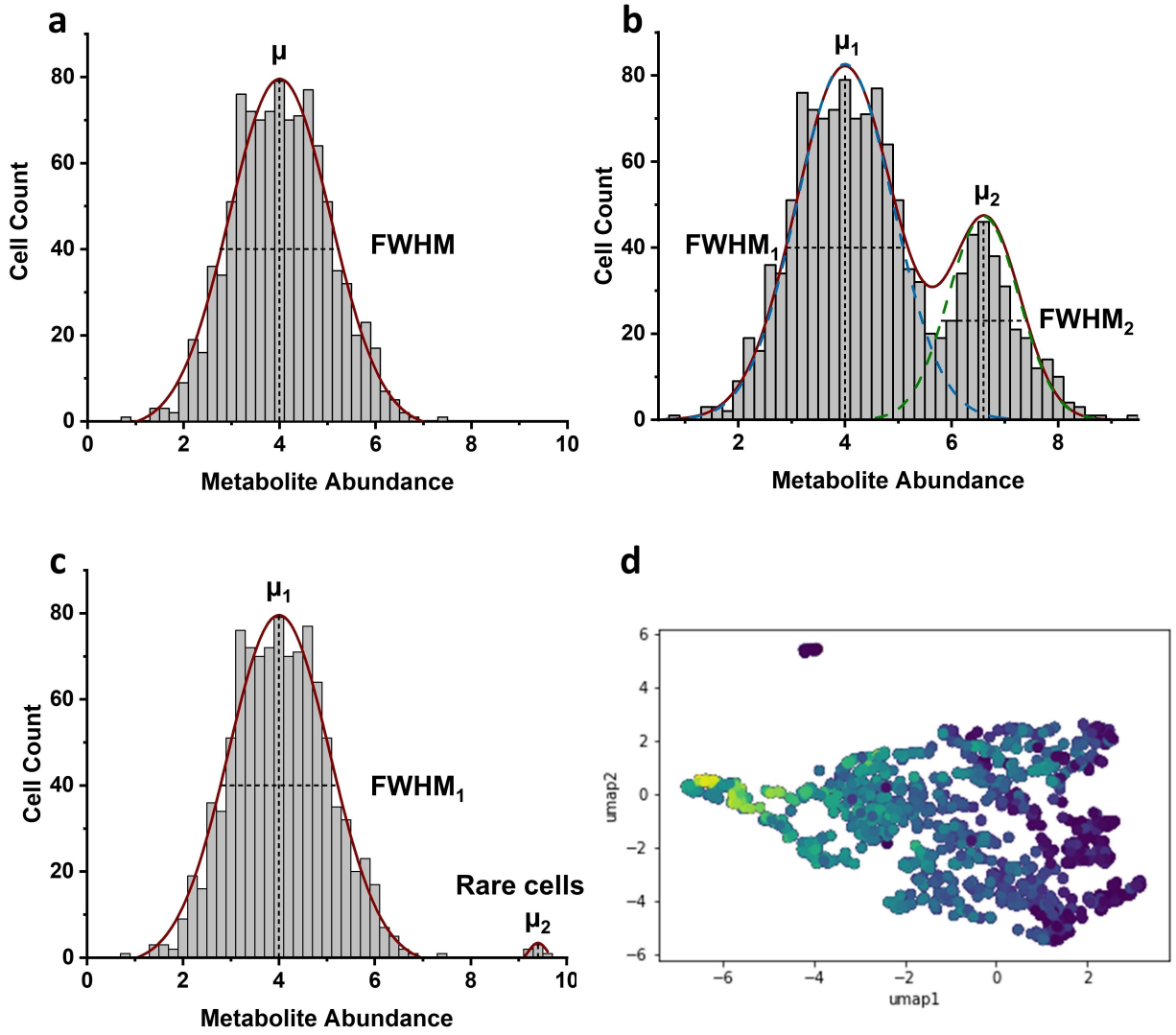

Figure 3. a) Unimodal and b) bimodal abundance distributions of metabolites detected at single cell level. The blue and green dashed curves represent the deconvoluted metabolite distribution. c) Rare cells were identified based on their significantly different metabolomic profile from the rest of the cell population. d) Subpopulations established by UMAP projection based on fumarate abundances in *A. cepa* epidermal cells (n = 1084).[55] Adapted with permission from Ref. [55]. Copyright 2021 American Chemical Society.

cell populations were uncovered. Comparing wild-type yeast cells with ones treated with a glycolysis inhibitor drug (2-deoxy-D-glucose), and with mutant cells (ΔPFK2) lacking one of the isoenzymes in the glycolysis pathway (phosphofructokinase) by MAMS revealed the presence of two phenotypes with different fructose-1,6-bisphosphate levels in the drug-treated cell population.[30]

There is a growing number of comparative studies performed at the single cell level. For example, cellular heterogeneity changes between control and lipopolysaccharide (LPS) treated macrophages were investigated at the single cell level by MALDI-MS imaging.[31] Upon LPS stimulation, the abundances of selected phospholipids exhibited broader distributions with higher mean values.

2.3. Single cell physiology

A comprehensive view of cellular physiology can be obtained by capturing some vital metabolic parameters **(Opportunity 5)** of the cell. Important examples include the cellular energy available to support healthy functioning expressed by the adenylate energy charge (AEC = ([ATP] + 0.5[ADP])/([ATP] + [ADP] + [AMP])), as well as the redox state of the cell characterized by the reduced to oxidized glutathione ratio ([GSH/GSSG]). Single cell metabolomics enables the measurement of these parameters for every analyzed cell.[6] In hepatocyte cell cultures, administering rotenone, a metabolic modulator that shuts down the electron transport chain in the mitochondria, resulted in reduced ATP production and a major downshift in the AEC levels. Hepatocytes exposed to oxidative stress exhibited a downshift in the [GSH/GSSG] ratio.

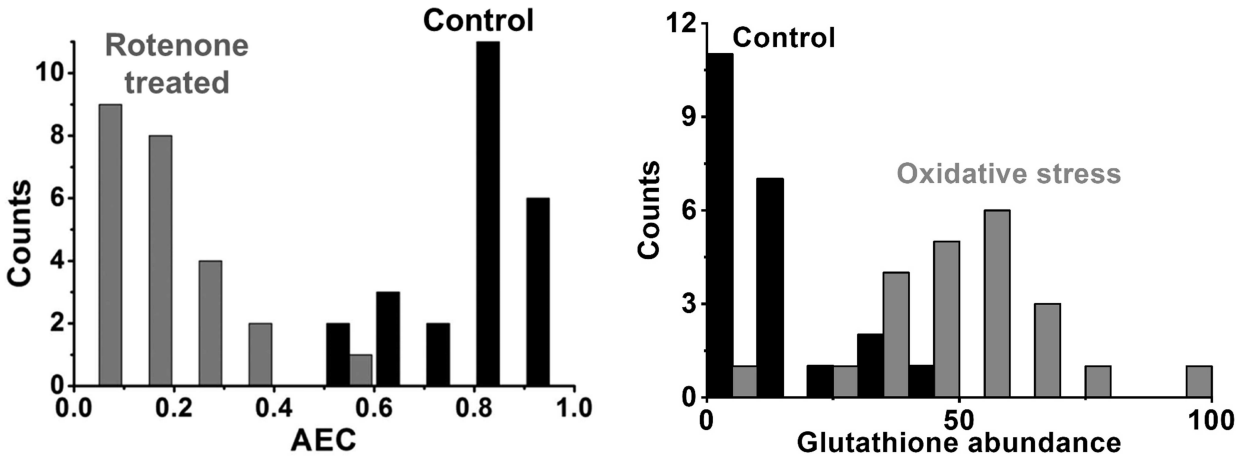

Figure 4. Metabolic states can be manifested in response to external perturbations. (Left panel) Healthy human hepatocytes (black bars, $n = 24$ cells) exhibit high adenylate energy charge, $AEC = 0.82 \pm 0.12$ with low metabolic noise, $\eta^2 = \sigma^2/\mu^2 = 0.021$. Rotenone treatment (gray bars, $n = 24$ cells) induces mitochondrial dysfunction resulting in apoptosis characterized by a low energy state, $AEC = 0.16 \pm 0.12$ and high metabolic noise, $\eta^2 = 0.562$.[6] Adapted with permission from Ref. [6]. Copyright 2015 American Chemical Society. (Right panel) Yeast cells ($n = 80$ cells) exposed to oxidative stress (gray bars) upregulate glutathione, a major redox buffer, compared to control cells raised in regular medium (black bars).[23] Adapted with permission from Ref. [23]. Copyright 2013 Wiley-VCH Verlag GmbH & Co. KGaA.

One of the early examples of recognizing cellular heterogeneity was the discovery and characterization of the cell cycle. Multiparametric flow cytometry measurements revealed fine details of cell cycle stages beyond the commonly recognized Gap 1 (G1), Synthesis (S), Gap 2 (G2), Mitosis (M) states, and the quiescent (G0) state.[32] Further distinctions were made for the five stages involved in mitosis: prometaphase, metaphase, anaphase, telophase, and cytokinesis. Although these stages were distinguished based on the synthesis and redistribution of DNA, they also implied differences in metabolic processes. Using capillary microsampling ESI-IMS-MS combined with fluorescence microscopy, distributions of AEC, [GTP]/[GDP], and [Hex-bis-P]/[Hex-P] ratios were compared for individual hepatocellular carcinoma cells at distinct mitotic stages.[33] Whereas the overall distribution of AEC for all miotic cells confirmed the presence of sufficient energy for proper cell functioning in all stages, a significant increase ($p = 0.005$) of AEC was observed between prometaphase (0.77 ± 0.13) and metaphase (0.93 ± 0.06). At the same time, the AEC metabolic noise decreased from $\eta^2 = 0.029$ to $\eta^2 = 0.004$, respectively.

Due to the extensive need for biosynthesis in cycling cells, they exhibit higher metabolic rates, e.g., elevated rate of glycolysis, than their quiescent (dormant) cells counterparts.[34] When cells in both states are present in a population, the distributions of certain metabolites can become bimodal. A potential example was observed in soybean root nodule cells hosting nitrogen fixing bacteroids transformed from soil bacteria.[18] In plant cells partially colonized by bacteroids, it was inferred that the latter were in a proliferating state, whereas in fully colonized plant cells, they were in a quiescent state induced by the limited volume available in the host cell. These two subpopulations provided a potential explanation for the observed bimodal NAD+ distributions.

2.4. Spatial metabolomics

Cells in the tissues of multicellular organisms are arranged in space to efficiently function together. This gives rise to cellular specialization into synergistic phenotypes. Recent advances in the **metabolomics of tissue embedded single cells have opened the door to explore these spatial arrangements (Opportunity 6)**. These methods grew out of the many modalities of MS imaging (MSI), including SIMS, MALDI, and f-LAESI.[35–39] These methods represent different tradeoffs between spatial resolution (~0.1 μm, ~5 μm, and ~30 μm, for SIMS, MALDI, and f-LAESI, respectively), degree of ion fragmentation (SIMS > MALDI ≈ f-LAESI), and the complexity of sample preparation (MALDI > SIMS > f-LAESI). Although the introduction of gas cluster ion beams (GCIBs) greatly reduces the degree of fragmentation in SIMS, for many small metabolites there is still significant ion degradation observed.[35] Nevertheless, subcellular tracking of metabolite levels by GCIB-SIMS provides unprecedented insight into spatial localization of biological processes, e.g., the first direct observation of metabolic channeling.[35] In an emerging indirect approach, quantitative spatial proteomics, based on multiplexed ion beam imaging (MIBI), is used to discern the enzymatic regulation of metabolic pathways.[40]

With the spatial capabilities available, **single cell transcript, protein, and metabolite atlases (Opportunity 7)** are being created for various tissues, organs, organisms, and their developmental stages. Currently, the Single Cell Expression Atlas (https://www.ebi.ac.uk/gxa/sc/home, last visited on 6/24/2021) covers transcripts for 18 species, and data on >5,000,000 cells. The Human Cell Atlas (https://www.humancellatlas.org/, last visited on 6/24/2021) and the Human Cell Landscape (https://db.cngb.org/HCL/, last visited on 6/24/2021) focus on the mapping of transcripts for the thousands of cell types present in the human body. The Human Protein Atlas (https://

www.proteinatlas.org/, last visited on 6/24/2021) captures the subcellular localization of transcripts and proteins and derives tissue/cell specific metabolic pathways. These atlases continuously curate new information, as more single cell proteomics and metabolomics data become available.

Additional research in single cell metabolomics will yield insights into cellular heterogeneity at the metabolite level, reveal the existence of hidden metabolic phenotypes, and illuminate the relationship between cell physiology, spatial distribution, and metabolic states.

3. Challenges

3.1. Cell size and cell manipulation

The small linear dimensions of single cells present major challenges in the manipulation and sampling of free floating (circulating) and tissue embedded cells. Cell sizes are strongly kingdom dependent. Unicellular organisms (e.g., bacteria) in the Kingdom Monera are 0.3 to 3 μm in diameter on average. Animal cells (Kingdom Animalia) are 10 to 30 μm in size, whereas plant cells (Kingdom Plantae) are in the 10 to 100 μm range. A direct comparison of bacterial and plant cell sizes is shown in Figure 2. The SEM image of *G. max* root nodule cells infected by *B. japonicum* indicates that the plant cell long and short axes are 16.7 μm and 13.6 μm, respectively, whereas a bacterial cell long and short axes are 2.4 μm and 0.55 μm, respectively. This means that cell manipulation, i.e., cell selection, isolation, and holding, requires specialized instrumentation for each cell type. As cell metabolism can be affected by mechanical perturbations, manipulation has to be kept at minimum.

The most commonly used single-cell isolation methods for free floating cells or cells dissociated from tissues include manual and robotic micromanipulation, fluorescence-activated cell sorting (FACS), and microfluidics.[41] For tissue embedded cells, laser capture microdissection (LCM), optical tweezers,[42] and in situ sampling by laser or ion beams are applicable. Methods are selected based on the cell size, sampling yield, throughput, and the degree of tolerable perturbation. Analyte loss during manipulation and sampling, as well as chemical perturbation are to be kept at a minimum.

In FACS, transcriptional and epigenetic alterations, as well as cell loss for tightly bound cells are common pitfalls. Microfluidic or lab-on-a-chip devices are high-throughput and sensitive platforms that offer high capture efficiency and minimized cell damage. For example, the rapid isolation of CTCs from unprocessed blood of a cancer patient using microfluidic device, allowed for *in situ* phenotypic and molecular characterization of trapped cells.[43] In LCM, cells are selected from a fixed tissue. Although it allows to keep spatial distribution information for single cells, it is a time-consuming process and requires expert personnel to harvest the cells.[41]

Keeping the sample under ambient conditions reduces metabolic stress and perturbations, and integrating the sampling step with analysis can be a gentle approach for single cell metabolomics.[44] For example, recently LAESI was employed for the sampling and analysis of single *Allium cepa* epidermal cells using a reflective objective to target selected cells for ambient *in situ* spatial metabolomics.[45] However, preserving cells under ambient conditions is not always trivial. Cells exposed to the open atmosphere can lose their native water content to evaporation if proper steps are not undertaken. For example, humidity-controlled enclosures can be used to minimize water evaporation from the cells.

3.2. Cell volume and metabolite pools per cell

The small linear dimensions of cells result in miniscule sample volumes, i.e., single cell analysis is severely volume limited. Cell volumes for the three kingdoms differ by orders of magnitude. For example, in *Escherichia coli*, *Homo sapiens*, and *Arabidopsis thaliana* the typical cell volumes are ~1 fL, 1 pL, and 20 pL, respectively. Considering the metabolite concentrations in these cells, ranges for their absolute amounts (pools) per cell can be estimated as 10^{-7} to 0.1 fmol for *E. coli*, 0.01 to 30 fmol for *H. sapiens*, and 2 to 10,000 fmol for *A. thaliana*.[46] A comparison of cell volumes for a *G. max* root nodule cell infected by *B. japonicum* in Figure 2 indicates 2430 fL and 0.6 fL for their volumes, respectively, i.e., the plant cell is ~4000 larger than the bacterial cell.

The small metabolite amounts per cell limit their detection to those with higher abundances or high ionization efficiencies. Therefore, improvement in LOD of the analysis platform, e.g., to the low amol range for human cells, is a common objective to maximize the chemical information obtained in single cell metabolomics.[47] Absolute metabolite concentrations are available for various cell types based on bulk cell culture measurements.[48] Table 1 summarizes the concentrations and absolute amounts (pools or reservoirs) of metabolites in single plant (*A. thaliana*), mammalian (iBMK), yeast (*S. cerevisiae*), and bacterial (*E. coli*) cells. The pools of different metabolites in a cell can span six orders of magnitude, e.g., from 0.5 zmol to 1 pmol, emphasizing the need for MS techniques with ultrahigh sensitivity and wide dynamic range. Some of the MS techniques applied for single cell and subcellular analysis exhibit LODs comparable to the amounts of metabolites with low abundance.

The relative ion intensities obtained for small metabolites in capillary microsampling ESI-IMS-MS of human hepatocytes showed that high abundance ions included glutamate, hexose phosphate, reduced glutathione, ADP, ATP, UDP-hexose, and UDP-N-acetylhexosamine.[6] According to Table 1, the corresponding metabolite pools per mammalian cell were ~64 fmol for glutamate, ~1 fmol for hexose phosphate, ~0.2 fmol for reduced glutathione, ~0.6 fmol for ADP, ~5 fmol for ATP, ~1.5 fmol for UDP-glucose, and ~9 fmol for UDP–N-acetylglucosamine. These relatively abundant metabolites regularly appeared in the mass spectra, whereas metabolites with low cellular abundances, e.g., cyclic-AMP at 0.0001 fmol and acetyl-CoA at 0.002 fmol, were missing from the spectra. Although relatively high metabolite amounts per cell are a prerequisite

Table 1. Concentrations and pools of metabolites in single plant (*Arabidopsis thaliana*), mammalian (iBMK), yeast (*S. cerevisiae*), and bacterial (*E. coli*) cells. Cell volumes are 20 pL, 1 pL, 0.05 pL, and 0.001 pL, respectively. Concentrations were established from bulk measurements in cell cultures or tissues.[48] Data for *A. thaliana* were for typical growth conditions.[62]

	Metabolites	KEGG ID	*A. thaliana*		Mammalian (iBMK)		Yeast		E. coli	
			Concentration [μM]	Pool [amol]	Concentration [μM]	Pool [amol]	Concentration [μM]	Pool [amol]	Concentration [μM]	Pool [amol]
Amino acids	Glutamine	C00064	7190	143800	17200	17200	35500	1775	3810	4
	Glutamate	C00025	1728	34560	63800	63800	39100	1955	96000	96
	Arginine	C00062	3447	68940	255	255	21800	1090	569	0.6
	Aspartate	C00049	861	17220	14900	14900	6290	314.5	4230	4
Energy rich molecules	AMP	C00020	21	420	42	42	81	4	281	0.3
	NAD^+	C00003	21	420	502	502	2440	122	2550	3
	ADP	C00008	19	380	569	569	488	24	555	0.6
	ATP	C00002	14	280	4670	4670	1930	96.5	9630	10
	$NADP^+$	C00006	12	240	28	28	183	9	2	0.002
	NADPH	C00005	3	60	65	65	221	11	121	0.1
	UTP	C00075			1760	1760	494	25	8290	8
	GTP	C00044			677	677	247	12	4870	5
	NADH	C00004			75	75	107	5	84	0.1
	Cyclic-AMP	C00575			0.1	0.1	0.4	0.02	35	0.04
Sugar derivatives	Glucose	C00031	1196	23920						
	Sucrose	C00089	1093	21860						
	Glucose-6-phosphate	C00092	266	5320	675	675	5310	265.5	7880	8
	UDP-glucose	C00029	79	1580	1530	1530	268	13	2500	2
	Fructose-6-phosphate	C00085	66	1320	97	97	2370	118.5	2520	3
	Fructose-1,6-bisphosphate	C00354	5	100	1520	1520	4000	200	15200	15
	ADP-glucose	C00498	0.2	4					4	0.004
	UDP–N-acetyl-glucosamine	C00043			8970	8970	1020	51	9240	9
	Hexose-phosphate				1070	1070	5860	293	8750	9
	Glyceraldehyde-3-phosphate	C00661			141	141	118	6	271	0.3
	Pentose-phosphate								1320	1
	Glucosamine-6-phosphate	C00352							1150	1
Organic acids	Malate	C00149	926	18520	1390	1390	925	46	1680	2
	Fumarate	C00122	651	13020	485	485	124	6	288	0.3
	Phosphoenolpyruvate	C00074	77	1540	12	12	29	1	184	0.2
	Citrate	C00158	75	1500	584	584	1490	74.5	1960	2
	Pyruvate	C00022	53	1060	5880	5880	9400	470	3660	4
	α-Ketoglutarate	C00026			797	797	848	42	443	0.4
	Oxaloacetate	C00036							0.5	0.0005
Others	Phosphate (orthophosphate)	C00009	5830	5830	49300	2465	23900	24		
	Glutathione	C00051	3090	3090	4300	215	16600	17		
	Acetyl-CoA	C00024	29	29	44	2	606	0.6		

for detection, the peak intensities also depend on ionization efficiencies that can vary widely for different metabolites. However, when the cellular metabolite amount falls below the LOD of the instrument for that compound, even 100% ionization efficiency is insufficient to result in detection.

3.3. Mass spectrometry related limitations

Due to the volume limited samples in single cell work, very **low LOD is** an **important** requirement for the mass spectrometer. This means that all main components of the instrument, sampling, ion source, analyzer, and detector, have to work at their best. For metabolites with micromolar to millimolar cellular concentrations (see Table 1), a mammalian cell contains amol to fmol amounts of analyte. Under ideal conditions, most high-end mass spectrometers can detect compounds in this domain. Ion sources must be able to efficiently produce ions from the metabolites and lipids in the cell. Several options have demonstrated single cell capabilities, including SIMS, ESI, MALDI, f-LAESI, and LDI from silicon nanopost arrays (NAPA).[6,15,23,35–37,49–50] High ionization efficiency goes a long way to identify metabolites even in microbial cells. For example, LDI from NAPA with an 800 zmol LOD, detected and putatively identified 24 metabolites in a yeast cell of ~30 fL in volume.[23] Time-of-flight (TOF) systems stand out as the most commonly used analyzers due to their very high ion transmission and short (sub-millisecond) acquisition time. In some applications, orbitrap and Fourier transform-ion cyclotron resonance (FT-ICR) analyzers are used because of their excellent mass resolution that can exceed 1,000,000 for the latter. This presents opportunities for the discovery of elemental formulas from a single cell even for unknown metabolites.[18]

Metabolomics for large cell populations heavily relies on the combination of separation methods with MS. This option is limited for single cells, because there are very few separation methods capable of handling samples with such a small volume. Capillary electrophoresis with ESI-MS has been used to explore metabolites in neuronal phenotypes.[51] Another option, ion mobility separation (IMS), moves the process past the ion source. This allows for low sample losses and very fast separation times, typically on the millisecond timescale but the resolution of separation is low.[6] Emerging IMS modalities, e.g., structures for lossless manipulations (SLIM), have achieved significantly improved resolution and demonstrated the separation of structural isomers.[52] As new IMS systems strive to achieve higher resolution at the expense of longer separation times, they might limit the throughput of single cell metabolomics.

Due to in-source fragmentation, the presence of structural isomers, or quasi-isobaric ions, the lack of separation in single cell analysis can result in the **misannotation of metabolites**.[19] For example, in-source decay of ATP can result in ADP, AMP, adenosine, and adenine. This not only creates ions not necessarily present in the cell at detectable levels but can also dramatically skew their biological abundances. The combination of new generation IMS with MS is expected to mitigate these limitations.

To achieve the statistical characterization of heterogeneity in metabolic cell states, numerous cells must be analyzed, and for that, **high-throughput** techniques are needed. Currently, only a few MS techniques are capable of high-throughput single-cell analysis. These include single-cell printer liquid vortex capture (SCP-LVC) MS at 1440 cells/h, optical microscopy combined with MALDI-MS at 1000 cells/h, and f-LAESI-MS at 62 cells/h.[53–55] Patterning isolated single cells on a surface followed by SIMS or MALDI-MS imaging also enable high throughput, although the time required for sample preparation and cell patterning can create a significant overhead.[30,56]

3.4. Half-life and diffusion of metabolites

Cellular metabolism continuously synthesizes and degrades every metabolite through enzymatic reactions. Some compounds also enter the cell from the environment, and some others are excreted into the extracellular space. Therefore, the pool of a metabolite present in the cell (see examples in Table 1) is being replaced at a net rate linked to the rates of synthesis and degradation, and for some, to incorporation and excretion. Turnover rates are most conveniently expressed through their inverse as half-life, $t_{1/2}$, that is defined as the time it takes to replace half of the pool for a particular compound. This is an important metric for single cell analysis because it indicates how quickly the metabolic processes must be quenched to minimize distortions to the measured analyte levels. For example, the half-lives for some slowly cycling metabolites, e.g., phosphatidylcholines (PC), in single hepatocytes were determined to be $t_{1/2}(\mathrm{PC(16:0/16:0)}) = 18.3 \pm 1.4$ h and $t_{1/2}(\mathrm{PC(16:0/16:1)}) = 21.0 \pm 1.4$ h.[6] However, for fast cycling metabolites, e.g., ATP, the half-lives are much shorter, $t_{1/2}(\mathrm{ATP}) \approx 5$ s, requiring rapid quenching.[46] Quenching of metabolism is most commonly accomplished by dramatically slowing down the enzymatic reactions by flash freezing, or by denaturing the enzymes using organic solvents, acids, or heat treatment.

Another factor that can distort the measured cellular abundances of metabolites is their diffusion in the sample. Displacement of molecules, driven by concentration gradients, can be characterized by the diffusion length, $x = (2Dt)^{1/2}$, where D is the diffusion coefficient, and t is time. For small molecules in human tissue at room temperature, $D \approx 10^{-6}$ cm^2/s, thus in 1 min they are displaced by ~110 μm. Considering that the average linear dimension for human cells is ~15 μm, this corresponds to a molecular displacement of more than 7 cell diameters.[57] Cryogenic sample preparation or conservation are often used to maintain the original spatial distributions.[35]

Minimizing the time and sample processing between a live cell and its analysis goes a long way to reduce artifacts due to metabolite turnover and diffusion. Recently developed ambient-ionization MS methods, including f-LAESI, capillary microsampling, single-probe MS, nano-DESI, and laser desorption ionization droplet delivery, offer low perturbation to cells in their native environment.[39,55,58]

3.5. Data analysis and integration

Data analysis in single cell metabolomics presents significant challenges due to **low-to-marginal signal intensities**, the **multidimensional nature of the mass spectra**, and the **large** and increasing **number of cells analyzed**. Solutions for similar issues have been introduced for single cell transcriptomics. Large sets of mass spectra with marginal signal intensities mean that some of the low intensity peaks are not present in all spectra. Multiple missing value imputation techniques have been proposed and tested for these scenarios including the promising quantile regression imputation of left-censored data (QRILC) approach.[59] Commonly used techniques for data reduction by multivariate statistical analysis of high-dimensional single cell omics datasets include the t-SNE and UMAP methods.[26] Artificial intelligence and machine learning are beginning to have an impact on both the extraction of marginal signal from the spectra[60] and the uncovering of hidden structures in the large single cell datasets.[61] Integration of single cell metabolomics with single cell proteomics and transcriptomics to produce the systems biology of a functioning cell is in its infancy. The complexities of this data integration are sure to create new computational challenges.

4. Conclusions

Emerging techniques in MS for volume-limited samples are laying the foundation for single cell metabolomics. With the development of high-throughput methods, they allow the determination of abundance distributions for hundreds of metabolites over cell populations of increasing sizes. Capturing metabolic heterogeneity, e.g., in the form of metabolic noise, can reveal the tightness of regulation for the levels of particular metabolites in complex pathway networks. Finding multimodal abundance distributions can lead to the discovery of latent subpopulations and hidden phenotypes primarily manifested in different metabolite levels.

Future developments in this field strongly depend on advances in MS technology, including the sensitivity of ionization methods and mass-analysis, the throughput of cell sampling, and the ability to perform the analysis with minimal perturbation of the cell. The improving performance of ion mobility separation methods is key for high throughput distinction of isobaric species, e.g., structural isomers. Accurate determination of the various metabolite levels, preferably via absolute quantitation, is a major remaining challenge in the field. Spatial metabolomics promises to explore how single cells in an organ work together for functional outcomes. New approaches are needed to directly analyze tissue embedded cells to fulfill this promise.

Acknowledgments

This work is supported by the U.S. National Science Foundation, Plant Genome Program; Division of Integrative Organismal Systems, Grant/Award Number: IoS-1734145.

Conflict of Interest

The authors declare no conflict of interest.

Keywords: mass spectrometry · metabolomics · proteomics · single-cell analysis · spatial distributions

[1] Y. Taniguchi, P. J. Choi, G. W. Li, H. Y. Chen, M. Babu, J. Hearn, A. Emili, X. S. Xie, *Science* **2010**, *329*, 533–538.
[2] S. S. Rubakhin, E. V. Romanova, P. Nemes, J. V. Sweedler, *Nat. Methods* **2011**, *8*, S20-S29.
[3] S. S. Rubakhin, E. J. Lanni, J. V. Sweedler, *Curr. Opin. Biotechnol.* **2013**, *24*, 95–104.
[4] S. J. Altschuler, L. F. Wu, *Cell* **2010**, *141*, 559–563.
[5] C. H. Johnson, J. Ivanisevic, G. Siuzdak, *Nat. Rev. Mol. Cell Biol.* **2016**, *17*, 451–459.
[6] L. Zhang, A. Vertes, *Anal. Chem.* **2015**, *87*, 10397–10405.
[7] T. H. Ong, D. J. Kissick, E. T. Jansson, T. J. Comi, E. V. Romanova, S. S. Rubakhin, J. V. Sweedler, *Anal. Chem.* **2015**, *87*, 7036–7042.
[8] P. M. Strzelecka, A. M. Ranzoni, A. Cvejic, *Dis. Model. Mech.* **2018**, *11*, dmm036525.
[9] L. Armbrecht, P. S. Dittrich, *Anal. Chem.* **2017**, *89*, 2–21.
[10] W. Y. Lu, X. Y. Su, M. S. Klein, I. A. Lewis, O. Fiehn, J. D. Rabinowitz, *Annu. Rev. Biochem.* **2017**, *86*, 277–304.
[11] A. H. Zhang, H. Sun, H. Y. Xu, S. Qiu, X. J. Wang, *OMICS* **2013**, *17*, 495–501.
[12] E. H. Ma, M. J. Verway, R. M. Johnson, D. G. Roy, M. Steadman, S. Hayes, K. S. Williams, R. D. Sheldon, B. Samborska, P. A. Kosinski, H. Kim, T. Griss, B. Faubert, S. A. Condotta, C. M. Krawczyk, R. J. DeBerardinis, K. M. Stewart, M. J. Richer, V. Chubukov, T. P. Roddy, R. G. Jones, *Immunity* **2019**, *51*, 856–870.
[13] D. S. Feng, T. R. Xu, H. Li, X. Z. Shi, G. W. Xu, *J. Anal. Test.* **2020**, *4*, 198–209.
[14] Y. Zhu, P. D. Piehowski, R. Zhao, J. Chen, Y. F. Shen, R. J. Moore, A. K. Shukla, V. A. Petyuk, M. Campbell-Thompson, C. E. Mathews, R. D. Smith, W. J. Qian, R. T. Kelly, *Nat. Commun.* **2018**, *9*, 882.
[15] B. Shrestha, A. Vertes, *Anal. Chem.* **2009**, *81*, 8265–8271.
[16] L. Z. Samarah, T. H. Tran, G. Stacey, A. Vertes, *Anal. Chem.* **2020**, *92*, 7299–7306.
[17] L. W. Zhang, N. Khattar, I. Kemenes, G. Kemenes, Z. Zrinyi, Z. Pirger, A. Vertes, *Sci. Rep.* **2018**, *8*.
[18] L. Z. Samarah, R. Khattar, T. H. Tran, S. A. Stopka, C. A. Brantner, P. Parlanti, D. Velickovic, J. B. Shaw, B. J. Agtuca, G. Stacey, L. Pasa-Tolic, N. Tolic, C. R. Anderton, A. Vertes, *Anal. Chem.* **2020**, *92*, 7289–7298.
[19] Y.-F. Xu, W. Lu, J. D. Rabinowitz, *Anal. Chem.* **2015**, *87*, 2273–2281.
[20] A. Oikawa, K. Saito, *Plant J.* **2012**, *70*, 30–38.
[21] P. S. Swain, M. B. Elowitz, E. D. Siggia, *Proc. Natl. Acad. Sci. USA* **2002**, *99*, 12795–12800.
[22] S. A. Stopka, R. Khattar, B. J. Agtuca, C. R. Anderton, L. Pasa-Tolic, G. Stacey, A. Vertes, *Front. Plant Sci.* **2018**, *9*, 1646.
[23] B. N. Walker, C. Antonakos, S. T. Retterer, A. Vertes, *Angew. Chem. Int. Ed.* **2013**, *52*, 3650–3653; *Angew. Chem.* **2013**, *125*, 3738–3741.
[24] A. W. DeVilbiss, Z. Y. Zhao, M. S. Martin-Sandoval, J. M. Ubellacker, A. Tasdogan, M. Agathocleous, T. P. Mathews, S. J. Morrison, *eLife* **2021**, *10*, e61980.
[25] Y. Abouleila, K. Onidani, A. Ali, H. Shoji, T. Kawai, C. T. Lim, V. Kumar, S. Okaya, K. Kato, E. Hiyama, T. Yanagida, T. Masujima, Y. Shimizu, K. Honda, *Cancer Sci.* **2019**, *110*, 697–706.
[26] E. Becht, L. McInnes, J. Healy, C. A. Dutertre, I. W. H. Kwok, L. G. Ng, F. Ginhoux, E. W. Newell, *Nat. Biotechnol.* **2019**, *37*, 38–44.

[27] K. Scupakova, F. Dewez, A. K. Walch, R. M. A. Heeren, B. Balluff, *Angew. Chem. Int. Ed.* **2020**, *59*, 17447–17450; *Angew. Chem.* **2020**, *132*, 17600–17603.
[28] P. P. Handakumbura, B. Stanfill, A. Rivas-Ubach, D. Fortin, J. P. Vogel, C. Jansson, *Sci. Rep.* **2019**, *9*, 1858.
[29] M. Ackermann, *Nat. Rev. Microbiol.* **2015**, *13*, 497–508.
[30] A. J. Ibanez, S. R. Fagerer, A. M. Schmidt, P. L. Urban, K. Jefimovs, P. Geiger, R. Dechant, M. Heinemann, R. Zenobi, *Proc. Natl. Acad. Sci. USA* **2013**, *110*, 8790–8794.
[31] B. Yang, N. H. Patterson, T. Tsui, R. M. Caprioli, J. L. Norris, *J. Am. Soc. Mass Spectrom.* **2018**, *29*, 1012–1020.
[32] Z. Darzynkiewicz, F. Traganos, M. R. Melamed, *Cytometry* **1980**, *1*, 98–108.
[33] L. W. Zhang, C. J. Sevinsky, B. M. Davis, A. Vertes, *Anal. Chem.* **2018**, *90*, 4626–4634.
[34] H. A. Coller, *FEBS Lett.* **2019**, *593*, 2817–2839.
[35] V. Pareek, H. Tian, N. Winograd, S. J. Benkovic, *Science* **2020**, *368*, 283–290.
[36] H. Tian, L. J. Sparvero, T. S. Anthonymuthu, W. Y. Sun, A. A. Amoscato, R. R. He, H. Bayr, V. E. Kagan, N. Winograd, *Anal. Chem.* **2021**, *93*, 8143–8151.
[37] S. Ganesh, T. Hu, E. Woods, M. Allam, S. Y. Cai, W. Henderson, A. F. Coskun, *Sci. Adv.* **2021**, *7*, eabd0957.
[38] A. R. Korte, M. D. Yandeau-Nelson, B. J. Nikolau, Y. J. Lee, *Anal. Bioanal. Chem.* **2015**, *407*, 2301–2309.
[39] B. Shrestha, J. M. Patt, A. Vertes, *Anal. Chem.* **2011**, *83*, 2947–2955.
[40] F. J. Hartmann, D. Mrdjen, E. McCaffrey, D. R. Glass, N. F. Greenwald, A. Bharadwaj, Z. Khair, S. G. S. Verberk, A. Baranski, R. Baskar, W. Graf, D. Van Valen, J. Van den Bossche, M. Angelo, S. C. Bendall, *Nat. Biotechnol.* **2021**, *39*, 186–197.
[41] Q. Zeb, C. Wang, S. Shafiq, L. Y. Liu, in *Single-Cell Omics: Technological Advances and Applications, Vol 1: Technological Advances* (Eds.: D. Barh, V. Azevedo), Elsevier, Amsterdam, **2019**, pp. 101–135.
[42] A. Keloth, O. Anderson, D. Risbridger, L. Paterson, *Micromachines* **2018**, *9*, 434.
[43] S. Ribeiro-Samy, M. I. Oliveira, T. Pereira-Veiga, L. Muinelo-Romay, S. Carvalho, J. Gaspar, P. P. Freitas, R. Lopez-Lopez, C. Costa, L. Dieguez, *Sci. Rep.* **2019**, *9*, 8032.
[44] A. Svatos, *Anal. Chem.* **2011**, *83*, 5037–5044.
[45] M. J. Taylor, S. Mattson, A. Liyu, S. A. Stopka, Y. M. Ibrahim, A. Vertes, C. R. Anderton, *Metabolites* **2021**, *11*, 200.
[46] L. W. Zhang, A. Vertes, *Angew. Chem. Int. Ed.* **2018**, *57*, 4466–4477; *Angew. Chem.* **2018**, *130*, 4554–4566.
[47] M. K. Passarelli, A. G. Ewing, *Curr. Opin. Chem. Biol.* **2013**, *17*, 854–859.
[48] J. O. Park, S. A. Rubin, Y. F. Xu, D. Amador-Noguez, J. Fan, T. Shlomi, J. D. Rabinowitz, *Nat. Chem. Biol.* **2016**, *12*, 482–489.
[49] L. Zhang, D. P. Foreman, P. A. Grant, B. Shrestha, S. A. Moody, F. Villiers, J. M. Kwake, A. Vertes, *Analyst* **2014**, *139*, 5079–5085.
[50] A. Amantonico, P. L. Urban, S. R. Fagerer, R. M. Balabin, R. Zenobi, *Anal. Chem.* **2010**, *82*, 7394–7400.
[51] P. Nemes, A. M. Knolhoff, S. S. Rubakhin, J. V. Sweedler, *Anal. Chem.* **2011**, *83*, 6810–6817.
[52] L. L. Deng, I. K. Webb, S. V. B. Garimella, A. M. Hamid, X. Y. Zheng, R. V. Norheim, S. A. Prost, G. A. Anderson, J. A. Sandoval, E. S. Baker, Y. M. Ibrahim, R. D. Smith, *Anal. Chem.* **2017**, *89*, 4628–4634.
[53] J. F. Cahill, J. Riba, V. Kertesz, *Anal. Chem.* **2019**, *91*, 6118–6126.
[54] L. Rappez, M. Stadler, S. Triana, R. Gathungu, K. Ovchinnikova, P. Phapale, M. Heikenwalder, T. Alexandrov, *Nat. Methods* **2021**, *18*, 799–805.
[55] S. A. Stopka, E. A. Wood, R. Khattar, B. J. Agtuca, W. M. Abdel-moulab, N. Y. R. Agar, G. Stacey, A. Vertes, *Anal. Chem.* **2021**, *93*, 9677–9687.
[56] L. Huang, Y. Chen, L. T. Weng, M. Leung, X. X. Xing, Z. Y. Fan, H. K. Wu, *Anal. Chem.* **2016**, *88*, 12196–12203.
[57] L. Z. Samarah, A. Vertes, *View* **2020**, *1*, 20200063.
[58] J. K. Lee, E. T. Jansson, H. G. Nam, R. N. Zare, *Anal. Chem.* **2016**, *88*, 5453–5461.
[59] R. M. Wei, J. Y. Wang, M. M. Su, E. Jia, S. Q. Chen, T. L. Chen, Y. Ni, *Sci. Rep.* **2018**, *8*, 663.
[60] Z. C. Liu, E. P. Portero, Y. R. Jian, Y. J. Zhao, R. M. Onjiko, C. Zeng, P. Nemes, *Anal. Chem.* **2019**, *91*, 5768–5776.
[61] T. Alexandrov, *Annu. Rev. Biomed. Data Sci.* **2020**, *3*, 61–87.
[62] S. Sato, S. Yanagisawa, *Plant Cell Physiol.* **2014**, *55*, 306–319.

Manuscript received: July 14, 2021
Revised manuscript received: October 19, 2021
Accepted manuscript online: October 20, 2021
Version of record online: November 8, 2021